

Journal of Biomedical Optics

SPIEDigitalLibrary.org/jbo

Sensitivity correction for the influence of the fat layer on muscle oxygenation and estimation of fat thickness by time-resolved spectroscopy

Etsuko Ohmae
Shinichiro Nishio
Motoki Oda
Hiroaki Suzuki
Toshihiko Suzuki
Kyoichi Ohashi
Shunsaku Koga
Yutaka Yamashita
Hiroshi Watanabe

Sensitivity correction for the influence of the fat layer on muscle oxygenation and estimation of fat thickness by time-resolved spectroscopy

Etsuko Ohmae,^{a,*} Shinichiro Nishio,^b Motoki Oda,^a Hiroaki Suzuki,^a Toshihiko Suzuki,^a Kyoichi Ohashi,^c Shunsaku Koga,^d Yutaka Yamashita,^a and Hiroshi Watanabe^b

^aHamamatsu Photonics K.K., Central Research Laboratory, 5000 Hirakuchi, Hamakita-ku, Hamamatsu, Shizuoka 434-8601, Japan

^bHamamatsu University School of Medicine, Department of Clinical Pharmacology and Therapeutics, 1-20-1 Handayama, Higashi-ku, Hamamatsu, Shizuoka 431-3192, Japan

^cOita University Faculty of Medicine, Department of Clinical Pharmacology and Therapeutics, 1-1 Idaigaoka, Hasama-machi, Yufu, Oita 879-5593, Japan

^dKobe Design University, Applied Physiology Laboratory, 8-1-1 Gakuennishi-machi, Nishi-ku, Kobe 651-2196, Japan

Abstract. Near-infrared spectroscopy (NIRS) has been used for noninvasive assessment of oxygenation in living tissue. For muscle measurements by NIRS, the measurement sensitivity to muscle (S_M) is strongly influenced by fat thickness (FT). In this study, we investigated the influence of FT and developed a correction curve for S_M with an optode distance (3 cm) sufficiently large to probe the muscle. First, we measured the hemoglobin concentration in the forearm ($n = 36$) and thigh ($n = 6$) during arterial occlusion using a time-resolved spectroscopy (TRS) system, and then FT was measured by ultrasound. The correction curve was derived from the ratio of partial mean optical path length of the muscle layer $\langle L_M \rangle$ to observed mean optical path length $\langle L \rangle$. There was good correlation between FT and $\langle L \rangle$ at rest, and $\langle L \rangle$ could be used to estimate FT. The estimated FT was used to validate the correction curve by measuring the forearm blood flow (FBF) by strain-gauge plethysmography (SGP_FBF) and TRS (TRS_FBF) simultaneously during a reactive hyperemia test with 16 volunteers. The corrected TRS_FBF results were similar to the SGP_FBF results. This is a simple method for sensitivity correction that does not require use of ultrasound. © 2014 Society of Photo-Optical Instrumentation Engineers (SPIE) [DOI: 10.1117/1.JBO.19.6.067005]

Keywords: near-infrared spectroscopy; time-resolved spectroscopy; plethysmography; muscle; hemoglobin; regional blood flow.

Paper 130910RR received Dec. 27, 2013; revised manuscript received May 13, 2014; accepted for publication May 15, 2014; published online Jun. 9, 2014.

1 Introduction

Near-infrared spectroscopy (NIRS) in the 700 to 900 nm region is useful for continuous and noninvasive assessment of oxygenation in living tissue. This method is based on the relatively high transparency of tissue to NIR light and the dependence of light absorption in this region on the hemoglobin (Hb) concentration in the tissue. The conventional continuous wave (CW) method is used to determine relative changes in Hb concentrations,¹⁻⁴ while time-resolved spectroscopy (TRS),⁵⁻⁸ phase modulation spectroscopy,⁹⁻¹² and broadband CW¹³ methods have been developed for quantitation of Hb concentrations in scattering media. However, NIRS signals also arise from other tissues, such as scalp, bone, and cerebrospinal fluid (CSF) for head measurements, and skin and fat for muscle measurements. The effects of multilayer tissue structures have been studied in simulations and phantom experiments.¹⁴⁻²³

For brain measurement, the effects of CSF and skin blood flow have been discussed.^{14,22,24} Many studies have shown the feasibility of assessing cerebral hemodynamics with NIRS.²⁵⁻²⁷ Increasing the optode spacing in experimental measurements can reportedly allow for brain signal detection by NIRS.²⁸⁻³⁰ The contribution of intracerebral tissue at 4 cm was ~70% in multidistance TRS measurement.^{31,32}

Furthermore, the TRS method with diffusion theory⁶ is reportedly affected less by skin blood flow than the CW method.³³⁻³⁵

For muscle measurements, the measurement sensitivity of muscle (S_M) is strongly influenced by the fat thickness (FT).³⁶⁻³⁸ There are considerable differences between individuals for FT, but fat tissue structure is not as complicated as brain tissue. A thicker fat layer decreases the partial mean optical path length of the muscle layer $\langle L_M \rangle$ and results in underestimation of muscle oxygenation. Therefore, quantitative comparison of NIRS data between individuals is difficult because of FT differences. Several approaches have been proposed to solve this problem, including proportional assessment using transient arterial occlusion,³⁹ time constant (τ), and the recovery time for parameters obtained by NIRS. Additionally, correction curves for S_M against FT have been estimated from $\langle L_M \rangle$ of Monte Carlo simulations.^{17,18,23}

In the TRS system, the distribution of mean optical path lengths $\langle L \rangle$ can be measured directly. Its temporal profile is analyzed using diffusion theory,⁶ which enables determination of the Hb concentration. In recent years, TRS has been applied in many areas, including monitoring of cerebral oxygen metabolism during surgery⁴⁰⁻⁴² and for neonates,^{43,44} bed side monitoring of subarachnoid hemorrhage,⁴⁵ the study of breast cancer,⁴⁶

*Address all correspondence to: Etsuko Ohmae, E-mail: etuko-o@crl.hpk.co.jp

and hemodynamic study of muscle.^{47,48} However, the fundamental issue described above has remained unresolved.

In this study, we used $\langle L_M \rangle / \langle L \rangle$ from TRS to develop a correction curve for S_M for changes in the muscle. The correction curve was validated by measuring forearm blood flow (FBF) simultaneously by TRS and strain-gauge plethysmography (SGP) during reactive hyperemia. We also studied the relationship between $\langle L \rangle$ and FT.

2 Materials and Methods

2.1 TRS

In this study, $\langle L \rangle$, the reduced scattering coefficient (μ'_s), the absorption coefficient (μ_a), the Hb concentration, and oxygen saturation (SO_2) were measured by TRS (TRS-10 for one channel,^{49,50} TRS-20 for two channels,^{47,51} Hamamatsu Photonics K.K., Hamamatsu, Japan).

Light pulses were emitted at 760, 795, and 830 nm, with full-width at half maximum of 100 ps, pulse rate of 5 MHz, and an average power of 200 μ W. The time-correlated single-photon counting (TCSPC) method was used to measure the temporal profile of detected photons.

2.2 TRS Data Analysis

$\langle L \rangle$ is the mean distance that photons travel through the tissue. This parameter is obtained directly from the mean time delay of the temporal profile by TRS measurement, assuming that the photons travel at a constant speed within the scattering medium.⁵² Usually, a deconvolution method is used to remove the influence of the measuring system, but this is a complicated process. Zhang et al. proposed a simple subtraction method for rapid and accurate calculation of $\langle L \rangle$ without deconvolution.⁵³ In this study, we used Zhang's method, which subtracts the center of gravity of the instrument response function (IRF) from that of the observed temporal profile. The validity of this method has been well proven numerically and experimentally.

The optical parameters (μ'_s and μ_a) were derived from the temporal profiles as described below. The behavior of a photon within scattering and absorption media, such as the human body, is expressed by the photon diffusion equation [Eq. (1)].⁶

$$\frac{1}{\nu} \frac{\partial}{\partial t} \phi(r, t) - D \nabla^2 \phi(r, t) + \mu_a \phi(r, t) = S(r, t), \quad (1)$$

where $\phi(r, t)$ is the diffuse photon fluence rate at position r and time t , D is the photon diffusion coefficient as expressed by $D = 1/3\mu'_s$, ν is the velocity of light within the media, and $S(r, t)$ is the light source.

Solutions using this equation are found under different boundary conditions. We used the solution of a semi-infinite homogeneous model with a zero boundary condition in reflectance mode⁶ for the TRS data analysis. In this solution, $R(d, t)$ is expressed by Eq. (2) as a function of the optode spacing, μ'_s , and μ_a .

$$R(d, t) = (4\pi D \nu)^{-\frac{3}{2}} z_0 t^{-\frac{5}{2}} \exp(-\mu_a \nu t) \exp\left(-\frac{d^2 + z_0^2}{4D\nu t}\right), \quad (2)$$

where d is the optode spacing and $z_0 = 1/\mu'_s$.

Using the weighted nonlinear least-squares method based on the Levenberg-Marquardt method, we fitted Eq. (2) for an instantaneous point source to the observed temporal profiles obtained from TRS and determined μ'_s and μ_a at each wavelength, while taking into account the effect of IRF.^{54,55} The weights for the least-squares calculations were obtained from Poisson distribution because the TRS data measured by TCSPC method have an error obeying the Poisson distribution.

We first assumed that absorption in the 700 to 900 nm range arose from oxygenated hemoglobin (oxyHb), deoxygenated hemoglobin (deoxyHb), and water. It is difficult to distinguish between myoglobin (Mb) and Hb because they have similar absorption spectra. In this study, most of the signals were assumed to arise from Hb, and the influence of Mb was ignored.^{56,57} The $\mu_{a\lambda}$ at the measured wavelengths λ (760, 795, and 830 nm) is expressed as shown in Eq. (3).

$$\begin{aligned} \mu_{a760 \text{ nm}} &= \epsilon_{\text{oxyHb}760 \text{ nm}} C_{\text{oxyHb}} + \epsilon_{\text{deoxyHb}760 \text{ nm}} C_{\text{deoxyHb}} \\ &\quad + \mu_{a\text{H}_2\text{O}760 \text{ nm}}, \\ \mu_{a795 \text{ nm}} &= \epsilon_{\text{oxyHb}795 \text{ nm}} C_{\text{oxyHb}} + \epsilon_{\text{deoxyHb}795 \text{ nm}} C_{\text{deoxyHb}} \\ &\quad + \mu_{a\text{H}_2\text{O}795 \text{ nm}}, \\ \mu_{a830 \text{ nm}} &= \epsilon_{\text{oxyHb}830 \text{ nm}} C_{\text{oxyHb}} + \epsilon_{\text{deoxyHb}830 \text{ nm}} C_{\text{deoxyHb}} \\ &\quad + \mu_{a\text{H}_2\text{O}830 \text{ nm}}, \end{aligned} \quad (3)$$

where $\epsilon_{m\lambda}$ is the molar extinction coefficient of substance m at wavelength λ and C_m is the concentration of substance m . The water absorption ($\mu_{a\text{H}_2\text{O}\lambda}$) was measured using a conventional spectral photometer (U-3500, Hitachi High-Technologies Corporation, Tokyo, Japan).

After subtracting the water absorption from μ_a at each wavelength, assuming the volume fraction of the water content was 60%,⁵⁸ we determined the concentrations of oxyHb and deoxyHb using the least-squares fitting method. The total concentration of hemoglobin (totalHb) and SO_2 were calculated from Eqs. (4) and (5).

$$\text{totalHb} = \text{oxyHb} + \text{deoxyHb}, \quad (4)$$

$$SO_2 = \frac{\text{oxyHb}}{\text{totalHb}} \times 100. \quad (5)$$

2.3 Estimation of S_M

We estimated S_M based on the method of Kohri et al.³¹ Figure 1 shows a model of fat and muscle layers during arterial occlusion. The optode spacing, d , was sufficient for photons to reach the muscle layer. The regions where light passed through were divided into a fat layer and a muscle layer. Each of these layers was homogeneous within the layer, and the two layers had different μ_a and μ'_s . FT was defined as the distance from skin surface to muscle, and the influence of the skin was ignored.³³⁻³⁵

The observed $\langle L \rangle$ was the sum of the partial mean optical path length of the fat layer $\langle L_F \rangle$ and $\langle L_M \rangle$, as follows:

$$\langle L \rangle = \langle L_F \rangle + \langle L_M \rangle. \quad (6)$$

Propagation of photons in the fat layer ($\langle L_F \rangle$) was regarded as the sum of the optical distances in two directions, from the

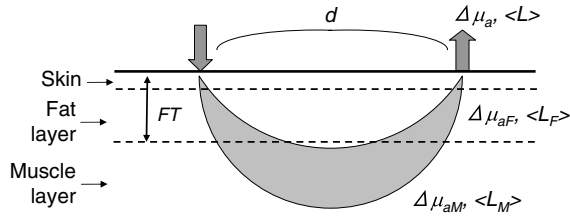


Fig. 1 Model of fat and muscle layers under arterial occlusion. The photon travels from the source to the detector in curved path. FT, fat thickness (skin + fat layer); $\langle L \rangle$, observed mean optical path length; $\langle L_F \rangle$, partial mean optical path length of the fat layer; $\langle L_M \rangle$, partial mean optical path length of the muscle layer; $\Delta\mu_a$, change in observed absorption coefficient; $\Delta\mu_{aF}$, change in absorption coefficient of the fat layer; $\Delta\mu_{aM}$, change in absorption coefficient of the muscle layer; d , optode spacing.

irradiation point to the muscle layer and from the muscle layer to the detection point. If $\langle L_F \rangle$ depends on FT, $\langle L_F \rangle$ is expressed using the differential path length factor of FT with an optode distance d (DPF_{fat} : partial mean path length for one direction per unit FT), as follows:

$$\langle L_F \rangle = 2 \times \text{FT} \times \text{DPF}_{\text{fat}}. \quad (7)$$

The modified Lambert-Beer's law for the two-layered structure is expressed as the summation of the optical density of each layer^{17,59} as follows:

$$\text{OD} = \langle L \rangle \times \mu_a + X = \langle L_F \rangle \times \mu_{aF} + \langle L_M \rangle \times \mu_{aM} + X, \quad (8)$$

where μ_a is the observed absorption coefficient; μ_{aF} and μ_{aM} are the absorption coefficients of the fat layer and the muscle layer, respectively; and X is the optical attenuation attributable to scattering.

When the absorption changes only in the muscle layer in arterial occlusion, the change in the observed absorption coefficient ($\Delta\mu_a$) is expressed as Eq. (9), where X is cancelled out.

$$\begin{aligned} \Delta\mu_a &= \frac{\Delta\text{OD}}{\langle L \rangle} = \frac{\langle L_M \rangle}{\langle L \rangle} \times \Delta\mu_{aM} = \frac{(\langle L \rangle - \langle L_F \rangle)}{\langle L \rangle} \times \Delta\mu_{aM} \\ &= S_M \times \Delta\mu_{aM}, \end{aligned} \quad (9)$$

where ΔOD is the change in the optical density, $\Delta\mu_{aM}$ is the change in the absorption coefficient of the muscle layer, and S_M is the measurement sensitivity to muscle with optode spacing d , which is expressed by dividing $\langle L_M \rangle$ by $\langle L \rangle$. The change in absorption coefficient in the fat layer was ignored because fat has very low blood volume and oxygen consumption.⁶⁰⁻⁶⁵

In general, deoxyHb has been used as an index of microvascular O_2 extraction in muscle studies by NIRS.^{48,66-69} The change in observed deoxyHb (ΔHb) showed an increase in arterial occlusion, and was expressed as a function of S_M and the change in deoxyHb of muscle (ΔHb_M) instead of $\Delta\mu_a$ and $\Delta\mu_{aM}$ [Eq. (10)], because ΔHb is directly proportional to $\Delta\mu_a$.

We assumed that the differences among individuals for muscle oxygen consumption (mVO_2) at rest were small and that the influence of FT on NIRS was larger than any differences among individuals.^{37,70} Then we determined DPF_{fat} and ΔHb_M so that the value of E in Eq. (11) was minimized using the least-squares method for all individuals.

$$\Delta\text{Hb} = S_M \times \Delta\text{Hb}_M = \frac{\langle L \rangle - 2 \times \text{FT} \times \text{DPF}_{\text{fat}}}{\langle L \rangle} \times \Delta\text{Hb}_M, \quad (10)$$

$$E = \sum_{i=1}^n \left\{ \Delta\text{Hb}(i) - \left[\frac{\langle L(i) - 2 \times \text{FT}(i) \times \text{DPF}_{\text{fat}}}{\langle L(i) \rangle} \times \Delta\text{Hb}_M \right] \right\}^2$$

($n = \text{number of volunteers}$).

(11)

If FT was known, S_M was estimated by dividing $\langle L_M \rangle$ by $\langle L \rangle$ using the determined DPF_{fat} , as shown in Eq. (12). Moreover, ΔHb divided by S_M provides an estimate of ΔHb_M .

$$S_M = \frac{\langle L_M \rangle}{\langle L \rangle} = \frac{\langle L \rangle - \langle L_F \rangle}{\langle L \rangle} = \frac{\langle L \rangle - 2 \times \text{FT} \times \text{DPF}_{\text{fat}}}{\langle L \rangle}. \quad (12)$$

2.4 Protocol

2.4.1 Arterial cuff occlusion test on the forearm and thigh

Informed consent was obtained from all subjects before the experiment. Arterial cuff occlusion on the forearm was performed on 21 male and 15 female healthy volunteers (37.6 ± 10.3 years of age), and on the thigh on six male healthy volunteers (23.9 ± 5.0 years of age). The optical probe for the forearm was attached to one point on the skin over the left brachioradialis muscle using the TRS-10 system. The optical probes for the thigh were attached to four places on the skin over the right vastus lateralis (VL) and the rectus femoris (RF) muscles at the distal and proximal sites using two TRS-20 systems. All optode distances were 3 cm. Sampling times for the forearm and thigh were 1 and 5 s, respectively. Arterial cuff occlusion tests were performed at rest with the subject in the supine position. TRS data recorded before occlusion were defined as the resting state. The occlusion cuff was placed on the upper forearm or the top of the thigh and connected to a pneumatically powered rapid inflator (E20, D. E. Hokanson Inc., Bellevue, Washington). The cuff on the forearm was inflated for 3 min at 250 mmHg and then deflated. The cuff on the thigh was inflated until the changes in deoxyHb and oxyHb plateaued at 250 mmHg, and then it was deflated. The FT at each optical measurement point was also measured by B-mode ultrasound (USD N-500, NIHON KOHDEN CORP., Tokyo, Japan or Logiq 400, GE-Yokogawa Medical Systems, Japan).

2.4.2 Simultaneous FBF measurement by SGP and TRS during reactive hyperemia

Informed consent was obtained from all subjects before the experiment. FBF at rest and after vascular endothelial stimulus by arterial occlusion was measured on the left forearm of 12 male and 4 female healthy volunteers (37.9 ± 10.5 years of age). These measurements were recorded by SGP and TRS-10 simultaneously. The venous occlusion method was used to measure FBF.^{57,71} FBF was observed as an increase in blood volume by interrupted venous flow and influx of arterial blood. By contrast, vascular endothelial stimulus by arterial occlusion leads to vasodilatation and an increase in FBF

(reactive hyperemia). The volunteers were in the supine position at rest. The cuff for venous occlusion was placed proximally on the left arm and connected to an automatic pneumatic inflator (E20, D. E. Hokanson Inc.) set to 40 mmHg.⁷²⁻⁷⁴ A second cuff was placed above the first cuff and connected to another pneumatic cuff inflator to provide arterial occlusion. To record measurements from the same region, wire strain-gauge for SGP (EC-5R, D. E. Hokanson Inc.) and an optical probe were placed in close proximity to each other on the skin over the brachioradialis muscle. Optode spacing was 3 cm, and the sampling time was 1 s. FT was estimated from the relationship between $\langle L \rangle$ and FT without measurement by ultrasound.

FBF measurements were performed with continuous cycles of 10 s of occlusion and 10 s of deflation of the venous cuff. First, three resting basal flow measurements were recorded. Next, rapid arterial occlusion of the left arm was executed by inflation of the arterial cuff for 3 min at 250 mmHg. This protocol stimulated reactive hyperemia. After the arterial cuff was suddenly deflated, FBF measurements by venous occlusion were repeated until the FBF value stabilized.

SGP is a popular method for measuring FBF using forearm volume changes during venous occlusion. Results from FBF obtained with SGP (SGP_FBF) are expressed in mL/min/100 mL. By contrast, FBF obtained with TRS (TRS_FBF) is defined as the maximum increase in totalHb per unit time (calculated as the slope of a linear fit of totalHb data over 5 s) during venous occlusion. Concentration changes in totalHb (ΔtHb) are expressed in $\mu\text{M/s}$ and are converted to mL/min/100 mL by taking into account the Hb concentration (14 g/dl) of blood and the molecular weight of Hb (64,500 g/mol), as shown in Eq. (13). For adjusting for the influence of fat, the obtained TRS_FBF results were corrected (cTRS_FBF) using Eq. (14).

$$\text{TRS_FBF} = \frac{\Delta tHb \times 64,500 \times 60}{14 \times 10^5}, \quad (13)$$

$$c\text{TRS_FBF} = \frac{\text{TRS_FBF}}{S_M}. \quad (14)$$

2.5 Statistical Analysis

Quantitative variances are expressed as mean \pm standard deviation. Comparisons of SGP_FBF and TRS_FBF before and after correction were analyzed using the squared Pearson's correlation coefficient (r^2) and the Bland-Altman test. In the Bland-Altman test, the precision of the bias was defined as two standard deviations of the mean difference, and the presence of fixed and proportional biases was investigated. The influence of FT on the TRS parameter was compared between forearm and thigh results by multiple regression analysis using a dummy variable. Statistical significance was defined with $P < 0.05$.

3 Results

Figure 2 shows a typical case (case 4, M, 28 years of age, VL at distal site) of TRS parameters ($\langle L \rangle$, μ'_s , μ_a at three wavelengths), the concentrations of oxyHb, deoxyHb, totalHb, and SO_2 , and the change in concentration of Hb during arterial occlusion of the thigh. During occlusion, although μ'_s at the three

wavelengths was almost constant, $\langle L \rangle$ and μ_a at 760 nm were different from that at the other wavelengths. A decrease in oxyHb and a simultaneous increase in deoxyHb were observed with depletion of local available O_2 , whereas totalHb remained almost constant. Similar trends were observed in the forearm data.

Figure 3 shows variations of $\langle L \rangle$, μ'_s , and μ_a at 795 nm, totalHb, and SO_2 in forearm and thigh under resting conditions plotted against FT obtained by ultrasound. The FT of the forearm was 0.49 ± 0.08 (range 0.34 to 0.64 cm), while FT of the thigh was 0.44 ± 0.11 (range 0.25 to 0.65 cm). As FT increased, $\langle L \rangle$ and μ'_s increased, and μ_a and totalHb decreased. Moreover, the relationships between FT and each of the TRS parameters, except for $\langle L \rangle$, were significantly different for the forearm and thigh results. By contrast, SO_2 was almost constant regardless of FT.

Figure 4 shows the relationship between FT and ΔHb and the change in SO_2 (ΔSO_2) during arterial occlusion for the forearm and four thigh positions (VL and RF at distal and proximal sites). Changes in these parameters were estimated in the first 2 min (selected part of totalHb is constant) during arterial occlusion to avoid the effect of Mb.^{56,57,75-77} When FT increased, ΔHb decreased and ΔSO_2 increased. Changes in these parameters in the thigh tended to be lower than in the forearm.

DPF_{fat} and ΔHb_M of the forearm and thigh were determined by Eq. (11) using FT, ΔHb , and $\langle L \rangle$ at 795 nm during rest (Table 1). These parameters were estimated in each position because changes in mVO_2 of the thigh depend on the position of the thigh during positron emission tomography (PET).⁷⁸ The estimated DPF_{fat} did not vary much (average 9.57 ± 0.66), but ΔHb_M was substantially different between the forearm and thigh. Figure 5 shows the relationship between FT and S_M . S_M was obtained from Eq. (12) using DPF_{fat} , $\langle L \rangle$ at 795 nm, and FT. S_M decayed exponentially with FT.

Figure 6(a) shows typical (case 11, M, 30 years of age) changes in the concentrations of oxyHb, deoxyHb, and totalHb during the forearm reactive hyperemia test. We determined TRS_FBF from the change in totalHb by venous occlusion. The FBF at the time of the first venous occlusion, which occurred immediately after release of arterial occlusion (250 mmHg), was excluded because the measurement conditions at this time differed from those at other times in the test. Figure 6(b) shows the results for SGP_FBF and TRS_FBF. Both these methods showed a large increase in FBF immediately after vascular endothelial stimulus compared with the resting state. The FBF then reduced gradually until rest. Additionally, we corrected TRS_FBF using the correction curve (Fig. 5) and obtained cTRS_FBF. FT was estimated from the relationship [Fig. 3(a)] between FT and $\langle L \rangle$ at 795 nm. FT was not measured by ultrasound in this protocol. The result for cTRS_FBF [Fig. 6(b)] was similar to that obtained by SGP_FBF. Table 2 shows $\langle L \rangle$ at 795 nm, FT estimated from $\langle L \rangle$, and S_M for each volunteer ($n = 16$). The estimated FT was 0.43 ± 0.08 (range 0.28 to 0.57 cm). S_M was 0.43 ± 0.05 (range 0.31 to 0.56).

Figure 7 shows the linear regression plot and the Bland-Altman plot of SGP_FBF, TRS_FBF, and cTRS_FBF. The slope improved from 0.28 [Fig. 7(a)] to 0.78 [Fig. 7(b)]. The correlation coefficient (r^2) improved slightly from 0.45 [Fig. 7(a)] to 0.53 [Fig. 7(b)] and showed good linearity. The bias and the precision (± 2 standard deviations) were 4.64 ± 6.14 mL/min/100 mL between SGP_FBF and

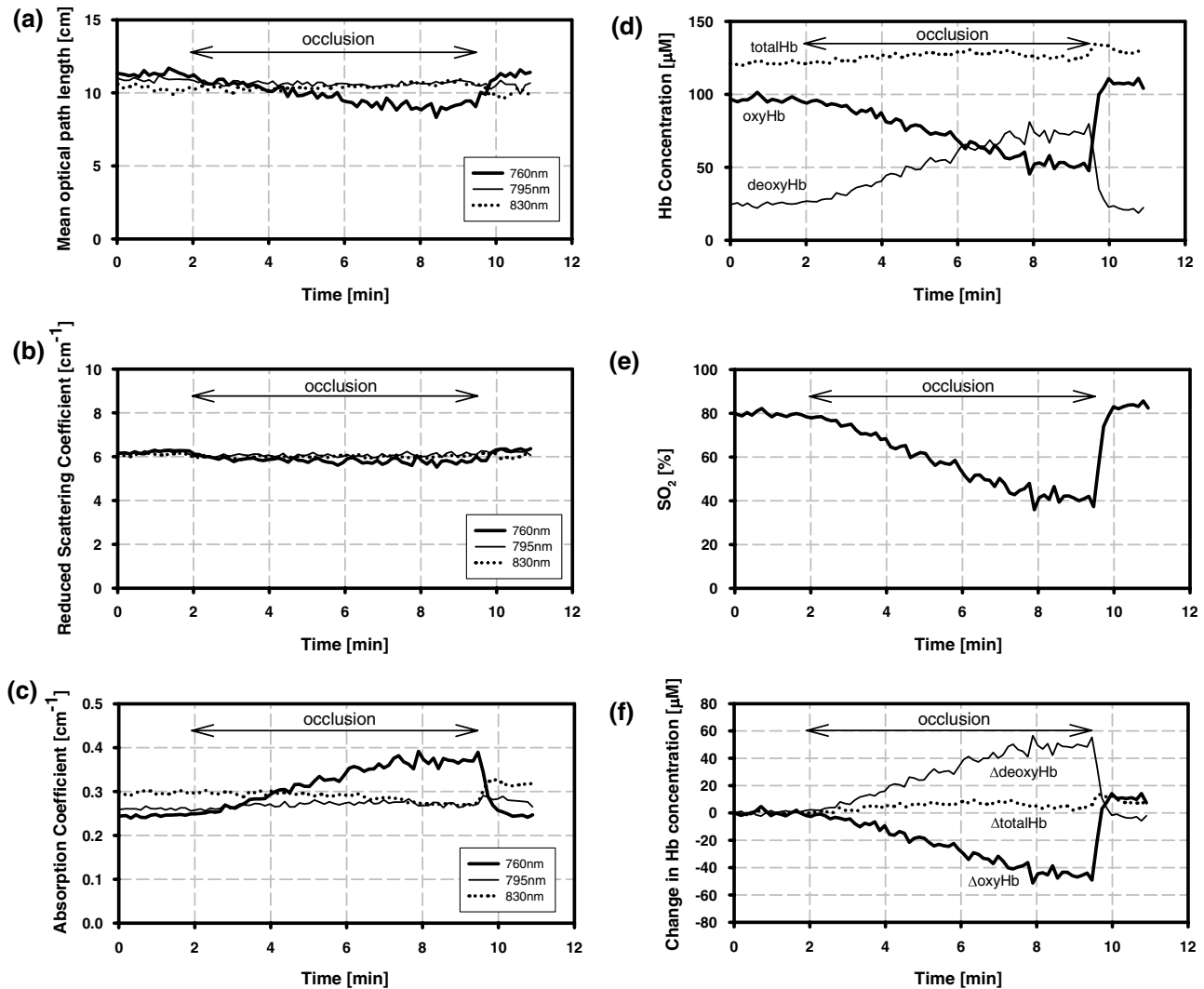


Fig. 2 Time course of time-resolved spectroscopy (TRS) parameters during arterial occlusion in a typical case [case 4, M, 28 years of age, vastus lateralis (VL) at distal site]: (a) $\langle L \rangle$, (b) μ'_s , (c) μ_a , (d) Hb concentration, (e) SO_2 , and (f) change in Hb concentration.

TRS_FBF [Fig. 7(c)], indicating the presence of fixed and proportional biases. By contrast, the bias and the precision between SGP_FBF and cTRS_FBF [Fig. 7(f)] were 0.48 ± 6.25 mL/min/100 mL, indicating the absence of fixed or proportional biases.

4 Discussion

4.1 Influence of FT on TRS Measurement Parameters

The influence of the fat layer on the NIRS signal has been reported for the CW method.^{36–38} Although the TRS method enables estimation of the absorption of the inner layer in media with two layers,^{79–84} we adapted a homogeneous model to facilitate practical application of TRS data analysis. The observed optical parameters (μ'_s and μ_a), $\langle L \rangle$, and the Hb concentration in the resting state were all influenced by FT (Fig. 3). As FT increased, μ'_s increased and μ_a decreased. Compared with muscle, fat causes more scattering and has a lower blood volume (absorption).^{64,65} With increasing FT, the forearm and thigh results showed different trends for μ'_s , μ_a ,

and totalHb. Similar results were reported in an earlier *in vivo* study at 800 nm,⁸⁵ where the forearm μ'_s was 6.9 cm^{-1} and μ_a was 0.23 cm^{-1} and the calf μ'_s was 8.9 cm^{-1} and μ_a was 0.17 cm^{-1} . In contrast to the other parameters, SO_2 was constant and not dependent on FT. This result shows that SO_2 in the fat layer and muscle layer are similar at rest. Even if the oxygen metabolism is different in the fat and muscle layers,^{37,56} a balance between oxygen supply and demand is maintained.

4.2 Estimation of DPF_{fat} and ΔHb_M from Arterial Occlusion

The change in SO_2 with arterial occlusion was affected by FT [Fig. 4(b)]. The change in deoxyHb showed the opposite trend to SO_2 with the change in FT [Fig. 4(a)]. The changes in SO_2 and deoxyHb were caused by an imbalance in O_2 consumption between the fat and muscle layers because oxygen metabolism is much higher in muscle than in fat.^{37,56}

We estimated DPF_{fat} and ΔHb_M from ΔHb and FT according to Eq. (11), assuming that ΔHb depends on oxygen metabolism in the muscle layer. ΔHb_M values differed greatly between the

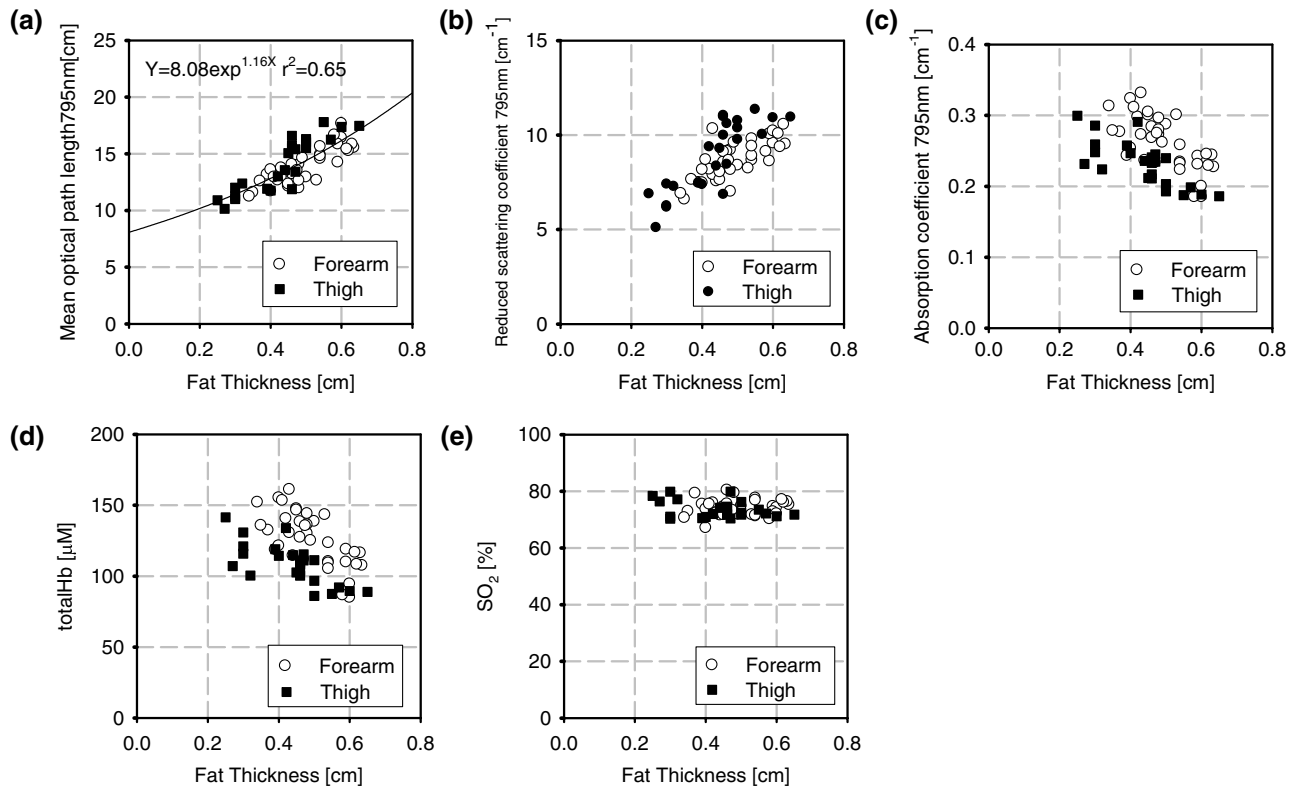


Fig. 3 The changes in (a) $\langle L \rangle$, (b) μ'_s , (c) μ_a , (d) totalHb, and (e) SO_2 of forearm and thigh at rest plotted against FT.

forearm and thigh (Table 1). We compared ΔHb_M with those obtained using conventional methods and basal metabolism, by converting ΔHb_M to mVO_2 values.¹⁸ These values were 0.20 and 0.11 ± 0.01 mL/100 g/min for the forearm and thigh, respectively. By comparison, a resting forearm mVO_2 of 0.15 mL/100 g/min was obtained by the conventional invasive Fick method,⁸⁶ and 0.16 mL/100 g/min by phosphorus magnetic resonance spectroscopy.^{87,88} These values are similar to that obtained in the present study. By contrast, earlier resting leg mVO_2 values of 0.18 mL/100 g/min from a muscle biopsy of human VL⁸⁹ and 0.19 mL/100 g/min from PET⁷⁸ were higher than our result. In the PET study, images suggested that oxygen consumption and blood volume near the surface

were lower than in deeper tissue.⁷⁸ Because NIRS measurements arise from relatively shallow tissue regions, the thigh mVO_2 obtained in the present study may have originated from a different tissue depth than the values obtained by the other methods. Johnson et al. reported that deeper tissue has more type 1 fibers than tissue closer to the surface in VL muscle.⁹⁰ By contrast, the cross-sectional area of the forearm is smaller than that of the thigh. Therefore, the forearm ΔHb_M may reflect the signal origin from the deeper tissue of the brachioradialis muscle.

We estimated the thigh ΔHb_M in four positions, specifically for the right VL and RF muscles at distal and proximal sites. These measurements were used to investigate the presence of spatially heterogeneous muscle oxygen metabolism. The thigh ΔHb_M at the proximal sites were smaller than those at the distal sites. Mizuno et al.⁷⁸ used PET to study thigh muscle after exercise and reported that mVO_2 changes became progressively larger as sampling gradually moved from proximal to distal sites in the muscle. By contrast, in the same study, mVO_2 at rest decreased as sampling moved from proximal to distal sites. Our result agreed with the trend observed by Mizuno et al.⁷⁸ after exercise. Arterial occlusion was performed at rest, but we recognize rapid change occurred in transient hypoxia in our experimental situation.

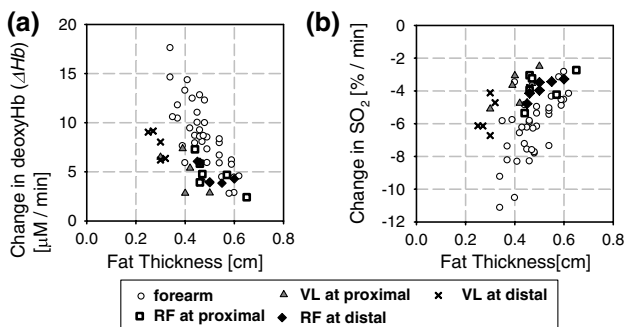


Fig. 4 Relationship between FT and the change in (a) deoxyHb and (b) SO_2 during arterial occlusion for the forearm and four positions [VL and rectus femoris (RF) at distal and proximal sites] in the thigh.

4.3 Correction Curve for Sensitivity to Muscle Oxygenation

Our correction curve showed lower sensitivity than the results of Niwayama et al.¹⁸ Their correction curve was obtained from a Monte Carlo simulation and *in vivo* measurement (ergometer

Table 1 DPF_{fat} and ΔHb_M determined using FT and ΔHb and ⟨L⟩ at 795 nm, μ_s' and μ_a at 795 nm, totalHb and SO₂ of each position at rest.

	<i>n</i>	DPF _{fat}	ΔHb _M (μM)	FT (cm)	ΔHb (μM)	⟨L⟩ _{795 nm} (cm)	μ _s ' _{795 nm} (cm ⁻¹)	μ _a _{795 nm} (cm ⁻¹)	TotalHb (μM)	SO ₂ (%)	
Forearm	36	8.94	23.77	0.47 ± 0.08	6.16 ± 2.46	13.93 ± 1.57	8.69 ± 1.02	0.2623 ± 0.037	125.9 ± 19.0	73.9 ± 2.8	
VL	Proximal	6	9.34	11.90	0.41 ± 0.07	4.85 ± 1.89	13.02 ± 1.61	8.31 ± 1.06	0.2532 ± 0.0353	115.9 ± 17.1	71.1 ± 0.6
	Distal	6	9.58	15.40	0.32 ± 0.07	7.11 ± 2.02	11.25 ± 0.79	6.43 ± 0.77	0.2505 ± 0.0270	116.0 ± 14.4	75.7 ± 3.7
Thigh	RF Proximal	6	9.32	12.14	0.51 ± 0.08	4.82 ± 1.66	15.66 ± 1.27	10.15 ± 0.98	0.2175 ± 0.0211	103.9 ± 11.3	74.0 ± 3.1
	Distal	6	10.67	13.81	0.51 ± 0.06	4.67 ± 1.05	16.43 ± 1.05	10.62 ± 0.73	0.2070 ± 0.0192	98.0 ± 8.8	73.5 ± 1.7

VL, vastus lateralis; RF, rectus femoris.

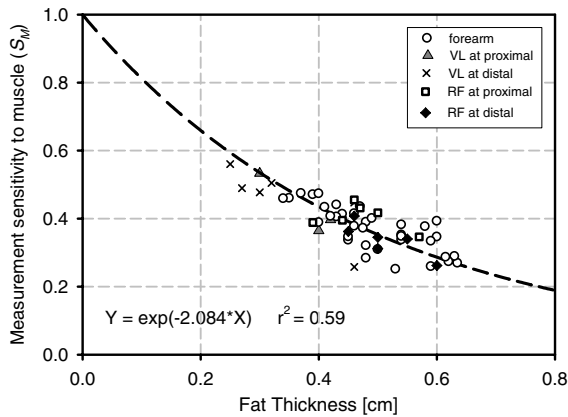


Fig. 5 Relationship between FT and *S_M* with 3 cm optode spacing estimated from experimental data in the forearm and four positions (VL and RF at distal and proximal sites) in the thigh.

exercise and ischemia tests) by the CW method. Specifically, the curve was normalized using the ratio of ⟨*L_M*⟩ to an FT of 0 mm, with ⟨*L_M*⟩ calculated from simulations using optical properties from the literature and *in vivo* data using DPF = 4.0. By comparison, our correction curve was derived from a ratio of ⟨*L_M*⟩ to ⟨*L*⟩ as described in Fig. 5. With TRS, ⟨*L*⟩ can be measured

directly without simulation or DPF. Because ⟨*L*⟩ is largely dependent on FT [Fig. 3(a)], the correction curve obtained using the observed ⟨*L*⟩ is expected to be more accurate than that of Niwayama, et al.¹⁸

4.4 Prediction of FT by ⟨*L*⟩

Interestingly, the relationship between ⟨*L*⟩ and FT was not significantly different between the forearm and thigh [Fig. 3(a)]. In a preliminary examination of this relationship, ⟨*L*⟩ at 10

Table 2 ⟨*L*⟩ at 795 nm, estimated FT from ⟨*L*⟩ and *S_M* in each volunteer (*n* = 16).

Case no.	⟨L⟩ _{795 nm} (cm)	Estimated FT (cm)	<i>S_M</i>
1	12.77	0.395	0.439
2	14.86	0.525	0.335
3	15.61	0.568	0.306
4	12.59	0.382	0.451
5	12.81	0.397	0.437
6	13.48	0.441	0.399
7	13.25	0.426	0.411
8	13.55	0.446	0.395
9	11.86	0.331	0.502
10	12.79	0.396	0.438
11	14.74	0.518	0.340
12	13.36	0.434	0.412
13	13.38	0.435	0.405
14	14.85	0.525	0.335
15	13.37	0.434	0.405
16	11.15	0.278	0.560
Average	13.40	0.433	0.410
Standard deviation	1.16	0.075	0.065

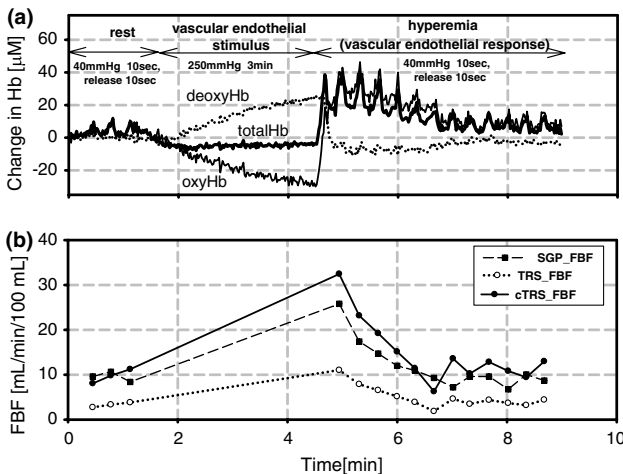


Fig. 6 Time course of changes in (a) concentration of oxyHb, deoxyHb, and totalHb and (b) SGP_FBF, TRS_FBF, and cTRS_FBF during forearm reactive hyperemia tests in a typical case (case 11, M, 30 years of age).

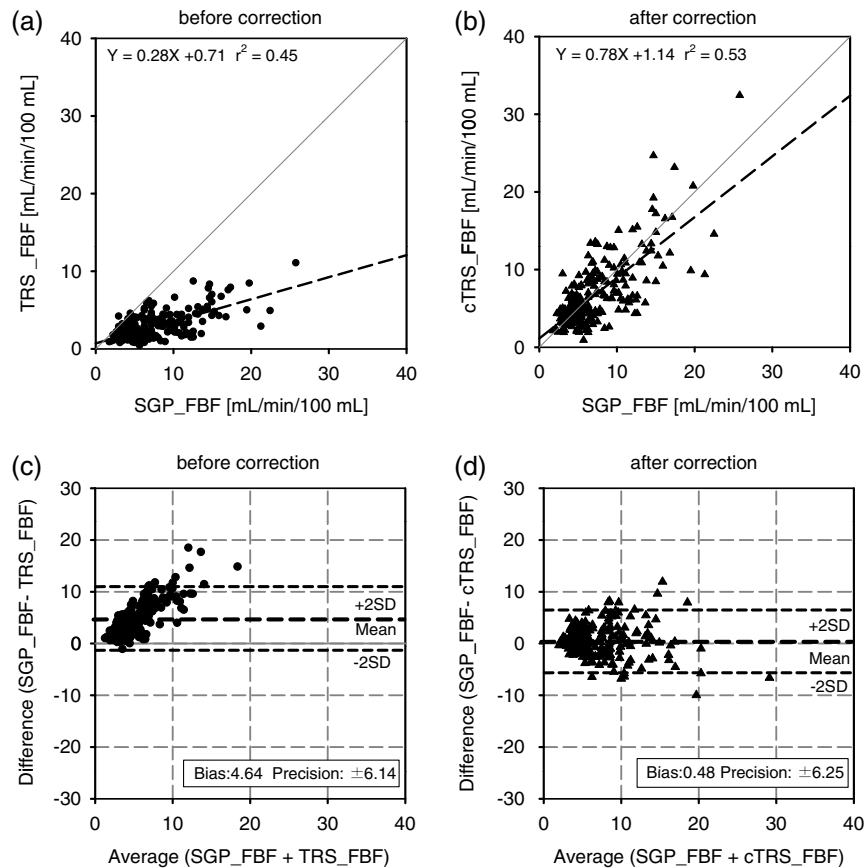


Fig. 7 Correlation between SGP_FBF and (a) TRS_FBF and (b) cTRS_FBF. Difference plots using Bland-Altman for SGP_FBF and (c) TRS_FBF and (d) cTRS_FBF.

positions on the skin over the VL and RF muscles of each volunteer ($n = 3$) obtained using TRS and FT values obtained by ultrasound (average 0.64 ± 0.08 cm, range 0.49 to 0.82 cm) were used. The relationship was consistent with the results of this study (data not shown). These results suggest that $\langle L \rangle$ could be used to estimate FT without requiring other methods, such as ultrasound or body fat calipers.

4.5 Validation of the Correction Curve

The correction curve was validated by comparing SGP_FBF and TRS_FBF results obtained during a reactive hyperemia test. The increase in blood volume from occlusion was ascribed to blood flow. In earlier studies without correction, NIRS_FBF results showed good agreement with SGP_FBF results,^{91–94} although the NIRS values were generally two-to-three times lower than those from SGP.^{56,86,92} In the present study, the slope of the curve for the comparison of the SGP_FBF and TRS_FBF results before correction was similar to these earlier reports. The reason NIRS_FBF is underestimated is because SGP reflects the total forearm blood flow of adipose, bone, skin, and skeletal muscle tissues, whereas NIRS reflects only the local flow in the region of interest and the signal primarily arises from small vessels.

In addition to the reason discussed above, we also demonstrated that FT had a large influence on NIRS data. cTRS_FBF results were similar to SGP_FBF results, and fixed and proportional biases disappeared (Fig. 7). The slope between cTRS_FBF and SGP_FBF improved from 0.28 to

0.78, and this result was in agreement with reports that hematocrit in capillaries is underestimated by $\sim 25\%$ compared with whole body results.^{56,95}

The TRS approach provides better reproducibility than SPG. Watanabe et al. reported that intrasubject variation from day-to-day with TRS was much lower than that with SGP, and SGP was susceptible to small body movements.⁹⁴ Therefore, the motion error in SGP should also be considered when comparing these techniques.

5 Conclusion

We determined S_M with a 3 cm optode spacing using arterial occlusion data obtained with a TRS system. A curve to correct for sensitivity to changes in muscle oxygenation was obtained using DPF_{fat} , FT, and $\langle L \rangle$. cTRS_FBF results corrected using this curve were similar to the SGP_FBF values in 16 volunteers. In addition, there was good correlation between $\langle L \rangle$ and FT in the experimental data. This result indicates FT could be estimated from $\langle L \rangle$ without ultrasound. TRS is a simple method to correct for sensitivity to muscle oxygenation without ultrasound. The correction curve is suitable for FT from 0.2 to 0.6 cm. Further work is required to extend the FT range and measurement position to allow for broader application of this method.

Acknowledgments

The authors would like to thank Mr. A. Hiruma for his constant support and encouragement.

References

1. M. Cope and D. T. Delpy, "System for long-term measurement of cerebral blood and tissue oxygenation on newborn infants by near infra-red transillumination," *Med. Biol. Eng. Comput.* **26**(3), 289–294 (1988).
2. P. F. Mason et al., "The assessment of cerebral oxygenation during carotid endarterectomy utilising near infrared spectroscopy," *Eur. J. Vasc. Surg.* **8**(5), 590–594 (1994).
3. T. J. Farrell, M. S. Patterson, and B. Wilson, "A diffusion theory model of spatially resolved, steady-state diffuse reflectance for the noninvasive determination of tissue optical properties in vivo," *Med. Phys.* **19**(4), 879–888 (1992).
4. S. Suzuki et al., "Tissue oxygenation monitor using NIR spatially resolved spectroscopy," *Proc. SPIE* **3597**, 582–592 (1999).
5. B. Chance et al., "Time-resolved spectroscopy of hemoglobin and myoglobin in resting and ischemic muscle," *Anal. Biochem.* **174**(2), 698–707 (1988).
6. M. S. Patterson, B. Chance, and B. C. Wilson, "Time resolved reflectance and transmittance for the non-invasive measurement of tissue optical properties," *Appl. Opt.* **28**(12), 2331–2336 (1989).
7. M. Oda et al., "A simple and novel algorithm for time-resolved multiwavelength oximetry," *Phys. Med. Biol.* **41**(3), 551–562 (1996).
8. Y. Yamashita et al., "Continuous measurement of oxy- and deoxyhemoglobin of piglet brain by time-resolved spectroscopy," *OSA Trends in Optics and Photonics* **22**, 205–207 (1998).
9. M. S. Patterson et al., "Frequency-domain reflectance for the determination of the scattering and absorption properties of tissue," *Appl. Opt.* **30**(31), 4474–4476 (1991).
10. J. B. Fishkin and E. Gratton, "Propagation of photon-density waves in strongly scattering media containing an absorbing semi-infinite plane bounded by a straight edge," *J. Opt. Soc. Am. A* **10**(1), 127–140 (1993).
11. S. Fantini, M. A. Franceschini, and E. Gratton, "Semi-infinite-geometry boundary problem for light migration in highly scattering media: a frequency-domain study in the diffusion approximation," *J. Opt. Soc. Am. B* **11**(10), 2128–2138 (1994).
12. Y. Tsuchiya and T. Urakami, "Frequency domain analysis of photon migration based on the microscopic Beer-Lambert law," *Jpn. J. Appl. Phys.* **35**(Part 1, No. 9A), 4848–4851 (1996).
13. H. Z. Yeganeh et al., "Broadband continuous-wave technique to measure baseline values and changes in the tissue chromophore concentrations," *Biomed. Opt. Express* **3**(11), 2761–2770 (2012).
14. M. Firbank, M. Schweiger, and D. T. Delpy, "Investigation of light pip-ing through clear regions of scattering objects," *Proc. SPIE* **2389**, 167–173 (1995).
15. E. Okada et al., "Theoretical and experimental investigation of near-infrared light propagation in a model of the adult head," *Appl. Opt.* **36**(1), 21–31 (1997).
16. E. Okada and D. T. Delpy, "Effect of scattering of arachnoid trabeculae on light propagation in the adult brain," presented at *Biomedical Optical Spectroscopy and Diagnostics*, paper ME3, Optical Society of America, Miami Beach, Florida (2000).
17. L. Lin et al., "Influence of a fat on muscle oxygenation measurement using near-IR spectroscopy: quantitative analysis based on two-layered phantom experiments and Monte Carlo simulation," *Front. Med. Biol. Eng.* **10**(1), 43–58 (2000).
18. M. Niwayama et al., "Quantitative measurement of muscle hemoglobin oxygenation using near-infrared spectroscopy with correction for the influence of a subcutaneous fat layer," *Rev. Sci. Instrum.* **71**(12), 4571–4575 (2000).
19. E. Okada and D. T. Delpy, "Near-infrared light propagation in an adult head model. I. Modeling of low-level scattering in the cerebrospinal fluid layer," *Appl. Opt.* **42**(16), 2906–2914 (2003).
20. E. Okada and D. T. Delpy, "Near-infrared light propagation in an adult head model. II. Effect of superficial tissue thickness on the sensitivity of the near-infrared spectroscopy signal," *Appl. Opt.* **42**(16), 2915–2922 (2003).
21. S. Misonoo and E. Okada, "Adult head modeling based on time-resolved measurement for NIR instrument," *Proc. SPIE* **4250**, 522–529 (2001).
22. Y. Fukui, Y. Ajichi, and E. Okada, "Monte Carlo prediction of near-infrared light propagation in realistic adult and neonatal head models," *Appl. Opt.* **42**(16), 2881–2887 (2003).
23. O. Sayli, E. B. Aksel, and A. Akin, "Crosstalk and error analysis of fat layer on continuous wave near-infrared spectroscopy measurements," *J. Biomed. Opt.* **13**(6), 064019 (2008).
24. T. Takahashi et al., "Influence of skin blood flow on near-infrared spectroscopy signals measured on the forehead during a verbal fluency task," *Neuroimage* **57**(3), 991–1002 (2011).
25. E. Keller et al., "Changes in cerebral blood flow and oxygen metabolism during moderate hypothermia in patients with severe middle cerebral artery infarction," *Neurosurg. Focus* **8**(5), e4 (2000).
26. J. T. Elliott et al., "Quantitative measurement of cerebral blood flow in a juvenile porcine model by depth-resolved near-infrared spectroscopy," *J. Biomed. Opt.* **15**(3), 037014 (2010).
27. R. Arora et al., "Preservation of the metabolic rate of oxygen in preterm infants during indomethacin therapy for closure of the ductus arteriosus," *Pediatr. Res.* **73**(6), 713–718 (2013).
28. P. W. McCormick et al., "Intracerebral penetration of infrared light. Technical note," *J. Neurosurg.* **76**(2), 315–318 (1992).
29. D. N. Harris et al., "NIRS in adults—effects of increasing optode separation," in *Oxygen Transport to Tissue XV*, P. Vaupel et al., Eds., Advances in Experimental Medicine and Biology, Vol. 345, pp. 837–840, Plenum Press, New York (1994).
30. T. J. Germon et al., "Optode separation determines sensitivity of near infrared spectroscopy to intra- and extracranial oxygenation changes," *J. Cereb. Blood Flow Metab.* **15**, 617 (1996).
31. S. Kohri et al., "Quantitative evaluation of the relative contribution ratio of cerebral tissue to near-infrared signals in the adult human head: a preliminary study," *Physiol. Meas.* **23**(2), 301–312 (2002).
32. E. Ohmae et al., "Cerebral hemodynamics evaluation by near-infrared time-resolved spectroscopy: correlation with simultaneous positron emission tomography measurements," *Neuroimage* **29**(3), 697–705 (2006).
33. A. H. Hielscher et al., "Time-resolved photon emission from layered turbid media," *Appl. Opt.* **35**(4), 719–728 (1996).
34. C. Sato et al., "Intraoperative monitoring of depth-dependent hemoglobin concentration changes during carotid endarterectomy by time-resolved spectroscopy," *Appl. Opt.* **46**(14), 2785–2792 (2007).
35. Y. Hoshi, "Towards the next generation of near-infrared spectroscopy," *Philos. Trans. A Math. Phys. Eng. Sci.* **369**(1955), 4425–4439 (2011).
36. S. Homma, T. Fukunaga, and A. Kagaya, "Influence of adipose tissue thickness on near infrared spectroscopic signal in the measurement of human muscle," *J. Biomed. Opt.* **1**(4), 418–424 (1996).
37. M. C. van Beekvelt et al., "Adipose tissue thickness affects in vivo quantitative near-IR spectroscopy in human skeletal muscle," *Clin. Sci. (Lond)* **101**(1), 21–28 (2001).
38. D. Geraskin, H. Boeth, and M. Kohl-Bareis, "Optical measurement of adipose tissue thickness and comparison with ultrasound, magnetic resonance imaging, and callipers," *J. Biomed. Opt.* **14**(4), 044017 (2009).
39. T. Hamaoka et al., "Near-infrared spectroscopy/imaging for monitoring muscle oxygenation and oxidative metabolism in healthy and diseased humans," *J. Biomed. Opt.* **12**(6), 062105 (2007).
40. E. Ohmae et al., "Clinical evaluation of time-resolved spectroscopy by measuring cerebral hemodynamics during cardiopulmonary bypass surgery," *J. Biomed. Opt.* **12**(6), 062112 (2007).
41. K. Yoshitani et al., "Clinical validity of cerebral oxygen saturation measured by time-resolved spectroscopy during carotid endarterectomy," *J. Neurosurg. Anesthesiol.* **25**(3), 248–253 (2013).
42. K. Yamazaki et al., "Cerebral oxygen saturation evaluated by near-infrared time-resolved spectroscopy (TRS) in pregnant women during caesarean section—a promising new method of maternal monitoring," *Clin. Physiol. Funct. Imaging* **33**(2), 109–116 (2013).
43. S. Ijichi et al., "Developmental changes of optical properties in neonates determined by near-infrared time-resolved spectroscopy," *Pediatr. Res.* **58**(3), 568–573 (2005).
44. K. Koyano et al., "The effect of blood transfusion on cerebral hemodynamics in preterm infants," *Transfusion* **53**(7), 1459–1467 (2013).
45. N. Yokose et al., "Bedside assessment of cerebral vasospasms after subarachnoid hemorrhage by near infrared time-resolved spectroscopy," in *Oxygen Transport to Tissue XXXI*, E. Takahashi and D. F. Bruley, Eds., Advances in Experimental Medicine and Biology, Vol. 662, pp. 505–511, Springer, New York (2010).
46. Y. Ueda et al., "Time-resolved optical mammography and its preliminary clinical results," *Technol. Cancer Res. Treat.* **10**(5), 393–401 (2011).

47. S. Koga et al., "Methodological validation of the dynamic heterogeneity of muscle deoxygenation within the quadriceps during cycle exercise," *Am. J. Physiol. Regul. Integr. Comp. Physiol.* **301**(2), R534–541 (2011).
48. L. M. Chin et al., "The relationship between muscle deoxygenation and activation in different muscles of the quadriceps during cycle ramp exercise," *J. Appl. Physiol.* **111**(5), 1259–1265 (2011).
49. M. Oda et al., "Near-infrared time-resolved spectroscopy system for tissue oxygenation monitor," *Proc. SPIE* **3597**, 611–617 (1999).
50. Y. Hoshi et al., "Resting hypofrontality in schizophrenia: a study using near-infrared time-resolved spectroscopy," *Schizophr. Res.* **84**(2–3), 411–420 (2006).
51. C. Sato et al., "Estimating the absorption coefficient of the bottom layer in four-layered turbid mediums based on the time-domain depth sensitivity of near-infrared light reflectance," *J. Biomed. Opt.* **18**(9), 097005 (2013).
52. D. T. Delpy et al., "Estimation of optical pathlength through tissue from direct time of flight measurement," *Phys. Med. Biol.* **33**(12), 1433–1442 (1988).
53. H. Zhang et al., "Simple subtraction method for determining the mean path length traveled by photons in turbid media," *Jpn. J. Appl. Phys.* **37** (Part 1, No. 2), 700–704 (1998).
54. K. Suzuki et al., "Quantitative measurement of optical parameters in the breast using time-resolved spectroscopy. Phantom and preliminary in vivo results," *Invest. Radiol.* **29**(4), 410–414 (1994).
55. A. Liebert et al., "Fiber dispersion in time domain measurements compromising the accuracy of determination of optical properties of strongly scattering media," *J. Biomed. Opt.* **8**(3), 512–516 (2003).
56. G. Yu et al., "Time-dependent blood flow and oxygenation in human skeletal muscles measured with noninvasive near-infrared diffuse optical spectroscopies," *J. Biomed. Opt.* **10**(2), 024027 (2005).
57. V. Quaresima et al., "Spatial distribution of vastus lateralis blood flow and oxyhemoglobin saturation measured at the end of isometric quadriceps contraction by multichannel near-infrared spectroscopy," *J. Biomed. Opt.* **9**(2), 413–420 (2004).
58. C. Fusch et al., "Body water, lean body and fat mass of healthy children as measured by deuterium oxide dilution," *Isotopenpraxis Isotopes Environ. Health Stud.* **29**(1–2), 125–131 (1993).
59. M. Hiraoka et al., "A Monte Carlo investigation of optical pathlength in inhomogeneous tissue and its application to near-infrared spectroscopy," *Phys. Med. Biol.* **38**(12), 1859–1876 (1993).
60. S. W. Coppack et al., "Postprandial substrate deposition in human forearm and adipose tissues in vivo," *Clin. Sci. (Lond)* **79**(4), 339–348 (1990).
61. P. Arner and J. Bulow, "Assessment of adipose tissue metabolism in man: comparison of Fick and microdialysis techniques," *Clin. Sci. (Lond)* **85**(3), 247–256 (1993).
62. K. N. Frayn, S. W. Coppack, and S. M. Humphreys, "Subcutaneous adipose tissue metabolism studied by local catheterization," *Int. J. Obes. Relat. Metab. Disord.* **17**(Suppl 3), S18–21; discussion S22 (1993).
63. L. Simonsen, J. Bulow, and J. Madsen, "Adipose tissue metabolism in humans determined by vein catheterization and microdialysis techniques," *Am. J. Physiol.* **266**(3 Pt 1), E357–365 (1994).
64. K. Matsushita, S. Homma, and E. Okada, "Influence of adipose tissue on muscle oxygenation measurement with an NIRS instrument," *Proc. SPIE* **3194**, 159–165 (1998).
65. C. R. Simpson et al., "Near-infrared optical properties of ex vivo human skin and subcutaneous tissues measured using the Monte Carlo inversion technique," *Phys. Med. Biol.* **43**(9), 2465–2478 (1998).
66. D. S. DeLorey, J. M. Kowalchuk, and D. H. Paterson, "Relationship between pulmonary O₂ uptake kinetics and muscle deoxygenation during moderate-intensity exercise," *J. Appl. Physiol.* **95**(1), 113–120 (2003).
67. B. Grassi et al., "Muscle oxygenation and pulmonary gas exchange kinetics during cycling exercise on-transitions in humans," *J. Appl. Physiol.* **95**(1), 149–158 (2003).
68. L. F. Ferreira et al., "Muscle capillary blood flow kinetics estimated from pulmonary O₂ uptake and near-infrared spectroscopy," *J. Appl. Physiol.* **98**(5), 1820–1828 (2005).
69. D. R. Jones et al., "Reply to Quaresima and Ferrari," *J. Appl. Physiol.* **107**, 372–373 (2009).
70. M. C. van Beekvelt et al., "In vivo quantitative near-infrared spectroscopy in skeletal muscle during incremental isometric handgrip exercise," *Clin. Physiol. Funct. Imaging* **22**(3), 210–217 (2002).
71. F. Harel et al., "Arterial flow measurements during reactive hyperemia using NIRS," *Physiol. Meas.* **29**(9), 1033–1040 (2008).
72. C. Casavola et al., "Blood flow and oxygen consumption with near-infrared spectroscopy and venous occlusion: spatial maps and the effect of time and pressure of inflation," *J. Biomed. Opt.* **5**(3), 269–276 (2000).
73. M. Annuk et al., "Impaired endothelium-dependent vasodilatation in renal failure in humans," *Nephrol. Dial. Transplant.* **16**(2), 302–306 (2001).
74. J. R. de Berrazueta et al., "Endothelial dysfunction, measured by reactive hyperaemia using strain-gauge plethysmography, is an independent predictor of adverse outcome in heart failure," *Eur. J. Heart Fail.* **12**(5), 477–483 (2010).
75. J. R. Wilson et al., "Noninvasive detection of skeletal muscle underperfusion with near-infrared spectroscopy in patients with heart failure," *Circulation* **80**(6), 1668–1674 (1989).
76. P. A. Mole et al., "Myoglobin desaturation with exercise intensity in human gastrocnemius muscle," *Am. J. Physiol.* **277**(1 Pt 2), R173–180 (1999).
77. R. S. Richardson et al., "Effect of mild carboxy-hemoglobin on exercising skeletal muscle: intravascular and intracellular evidence," *Am. J. Physiol. Regul. Integr. Comp. Physiol.* **283**(5), R1131–1139 (2002).
78. M. Mizuno et al., "Regional differences in blood flow and oxygen consumption in resting muscle and their relationship during recovery from exhaustive exercise," *J. Appl. Physiol.* **95**(6), 2204–2210 (2003).
79. A. Kienle et al., "Noninvasive determination of the optical properties of two-layered turbid media," *Appl. Opt.* **37**(4), 779–791 (1998).
80. J. Ripoll et al., "Recovery of optical parameters in multiple-layered diffusive media: theory and experiments," *J. Opt. Soc. Am. A Opt. Image Sci. Vis.* **18**(4), 821–830 (2001).
81. A. Sassaroli et al., "Performance of fitting procedures in curved geometry for retrieval of the optical properties of tissue from time-resolved measurements," *Appl. Opt.* **40**(1), 185–197 (2001).
82. F. Martelli, S. Del Bianco, and G. Zaccanti, "Procedure for retrieving the optical properties of a two-layered medium from time-resolved reflectance measurements," *Opt. Lett.* **28**(14), 1236–1238 (2003).
83. M. Shimada, Y. Hoshi, and Y. Yamada, "Simple algorithm for the measurement of absorption coefficients of a two-layered medium by spatially resolved and time-resolved reflectance," *Appl. Opt.* **44**(35), 7554–7563 (2005).
84. L. Gagnon et al., "Double-layer estimation of intra- and extracerebral hemoglobin concentration with a time-resolved system," *J. Biomed. Opt.* **13**(5), 054019 (2008).
85. S. J. Matcher, M. Cope, and D. T. Delpy, "In vivo measurements of the wavelength dependence of tissue-scattering coefficients between 760 and 900 nm measured with time-resolved spectroscopy," *Appl. Opt.* **36**(1), 386–396 (1997).
86. M. C. Van Beekvelt et al., "Performance of near-infrared spectroscopy in measuring local O₂ consumption and blood flow in skeletal muscle," *J. Appl. Physiol.* **90**(2), 511–519 (2001).
87. T. Hamaoka et al., "Noninvasive measures of oxidative metabolism on working human muscles by near-infrared spectroscopy," *J. Appl. Physiol.* **81**(3), 1410–1417 (1996).
88. T. Sako et al., "Validity of NIR spectroscopy for quantitatively measuring muscle oxidative metabolic rate in exercise," *J. Appl. Physiol.* **90**(1), 338–344 (2001).
89. R. C. Harris et al., "The effect of circulatory occlusion on isometric exercise capacity and energy metabolism of the quadriceps muscle in man," *Scand. J. Clin. Lab Invest.* **35**(1), 87–95 (1975).
90. M. A. Johnson et al., "Data on the distribution of fibre types in thirty-six human muscles. An autopsy study," *J. Neurol. Sci.* **18**(1), 111–129 (1973).
91. A. D. Edwards et al., "Measurement of hemoglobin flow and blood flow by near-infrared spectroscopy," *J. Appl. Physiol.* **75**(4), 1884–1889 (1993).

92. R. A. De Blasi et al., "Noninvasive measurement of forearm blood flow and oxygen consumption by near-infrared spectroscopy," *J. Appl. Physiol.* **76**(3), 1388–1393 (1994).
93. S. Homma et al., "Near-infrared estimation of O₂ supply and consumption in forearm muscles working at varying intensity," *J. Appl. Physiol.* **80**(4), 1279–1284 (1996).
94. H. Watanabe et al., "Assessment of forearm reactive hyperemia using near-infrared time resolved spectroscopy: a new tool to evaluate endothelial function," in *Proc. of Asian Symp. on BOPM*, Sapporo, pp. 164–165 (2002).
95. P. Vaupel, F. Kallinowski, and P. Okunieff, "Blood flow, oxygen consumption and tissue oxygenation of human tumors," *Adv. Exp. Med. Biol.* **277**, 895–905 (1990).

Biographies of the authors are not available.